Evaluation of RCC Defects in LESS Joggle Regions, Report 2

Randy Lee

Jacobs Engineering ESTS

NASA Marshall Space Flight Center

November, 2007

Mechanical and Physical Property Relationships in Carbon-Carbon

This report is in response to certain topics discussed during recent telecons regarding physical and mechanical testing of RCC components and attempts to explore possible correlations between relevant material properties. Direct correlations between carbon-carbon physical properties (density, porosity, matrix content, fiber volume) and mechanical strength attributes (ILT, flexural, shear) are not only possible, many have already been established. At one time, determination of simple flexural strength (and flex modulus) was the primary mechanical requirement for ACC and RCC/LESS test articles. Typical flexural failures are often multi-modal, usually breaking the 6" long specimens in tension on the back side while fibers on the crosshead side buckle in compression with occasional shearing near the middle of thick laminates (or laminates with weak planes). When the span is reduced to < 2", the failure mechanism is often dominated by interlaminar shearing between plies (i.e... short beam shear). Specimens of ACC (PAN-based Advanced Carbon-Carbon) typically fail along one plane near the center of the laminate while RCC (rayon-based Reinforced Carbon-Carbon) often exhibits primary and secondary shearing within the body of the laminate. However, during the early 1980's, an improved method for mechanically characterizing composite interlaminar nesting, ply-to-ply association and fiber-matrix adhesion was desperately needed for ACC... and RCC could only benefit from the effort that was forthcoming. After several months of development which included hundreds of trials and method refinement, my team developed and validated a specific ILT test procedure (flatwise tensile) that was eventually adopted as the standard ILT characterization technique for both ACC and RCC composites (this was the original modern ILT version implemented and used at LTV from that point onward). InterLaminar Tensile (referred to as 'across ply tensile' in the nozzle community) became the ultimate mechanical test for defining laminated 2-D composites across the board. There is no doubt that meaningful correlations between ILT values and other physical properties are essential and invaluable.

Hopefully, in some way or another, these experiences can help facilitate the current RCC investigation efforts, since several of the test concepts and characterization approaches under consideration have already been tried and proven (or disproven). Unfortunately, most of the physical notes and data I took with me when I left LTV were destroyed in a flood several years later. All I have at this point in time is a few remnants of the many issued reports and documents I generated during that period (and my memories). However, there are many points I recall very distinctly. In flat panel test regions, typical ILT ranges were 600–1200 psi for uncoated RCC-3 LESS panels, 300–900 psi for ACC-4 PAN laminates and 200–600 psi for 3-D ACC-4 PAN preform samples (experimental). It has always been obvious that the crenulated morphology of the LESS's carbonized rayon fibers contributed to relatively pronounced nesting between fabric planes while interlaminar nesting in PAN laminates was undesirably low and of course non-existent in 3-D preforms. After 3000° SiC conversion coating and sealing, ILT values drop anywhere from 40% to 70% with RCC producing the lowest decrease in strength and ACC the highest. For freshly manufactured product, typical post-coated ILT values for RCC-3 were generally in the 400–800 psi range and 200–600 psi for coated ACC . . . *in flat regions*. During this task, we tested many different adhesives and specimen configurations in efforts to optimize consistency in terms of failure mode and data spread. As reflected in the wide ranges given above, consistency in flatwise ILT failure loads leaves much to be desired. I do not recall the specific adhesive selected, I believe it was one of the Epon epoxies. Application of this method to coated specimens was also favorable since micrographs revealed that adhesive penetration into the coating phase was insignificant. We tested several specimen sizes and dimensions, including ½ to 1 inch squares, ½ to 1 inch circles and ½ to 1 by 1 to 2 inch rectangles. One might think that the square and circle shaped samples would produce the best results, but they didn't. Strangely, 1 by 2 inch specimens repeatedly gave the most consistent results. This configuration generated the fewest secondary moments as evidenced by single ply-to-ply interlaminar failures rather than those that peeled or ripped through several plies as was common with the other configurations. The 1" X 2" sample proved to be consistent even on various test machines including several Instrons, MTA, Tinius Olsen and Universal Test Machines. Ultimately, from these findings, we had a couple of pairs of special test fixtures made and a hundred pairs of steel test blocks fabricated like those illustrated in Figure 1 [1].

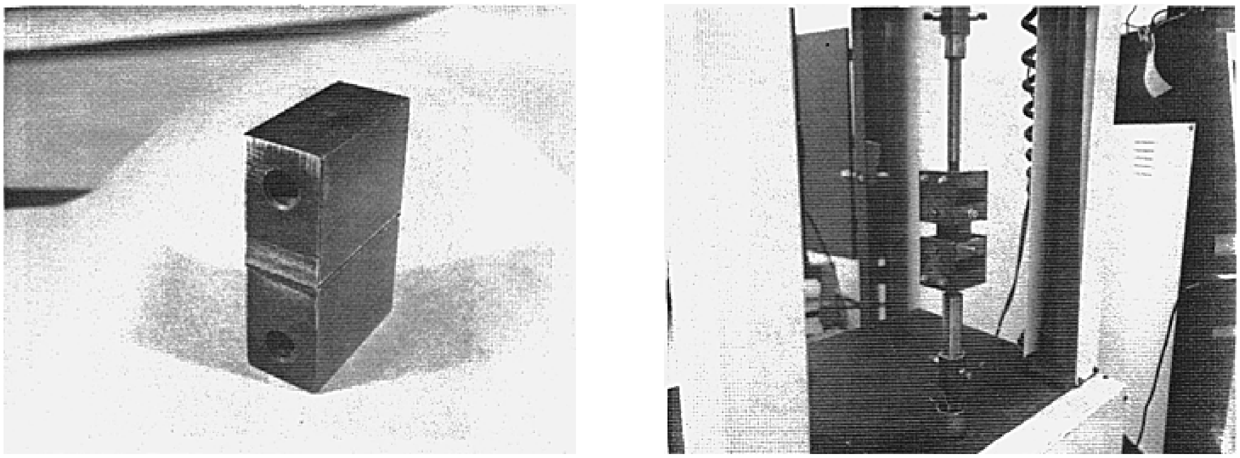

Figure 1. Left – Steel ILT test block configuration with 1 by 2 inch test sample mounted. Right – Mounted ILT test sample in a flexible loading fixture awaiting to be tested.

In spite of the rigorous optimization that was carried out during refinement of this technique, it was still obvious that undesirable moments were sometimes contributing to the failure mechanism. This was often reflected by the number of outliers in the data. Occasionally, the adhesive would fail at a low value indicating a poor bonding interface, while all the other samples in the test group mounted at the same time performed normally. I believe the ultimate bonding strength of the adhesive was upwards > 1500 psi. Figure 2 [1] gives an example of a normal failure (delam in the body of the sample) and an adhesive failure (implying either the sample was stronger than the adhesive or the adhesive bond was inadequate).

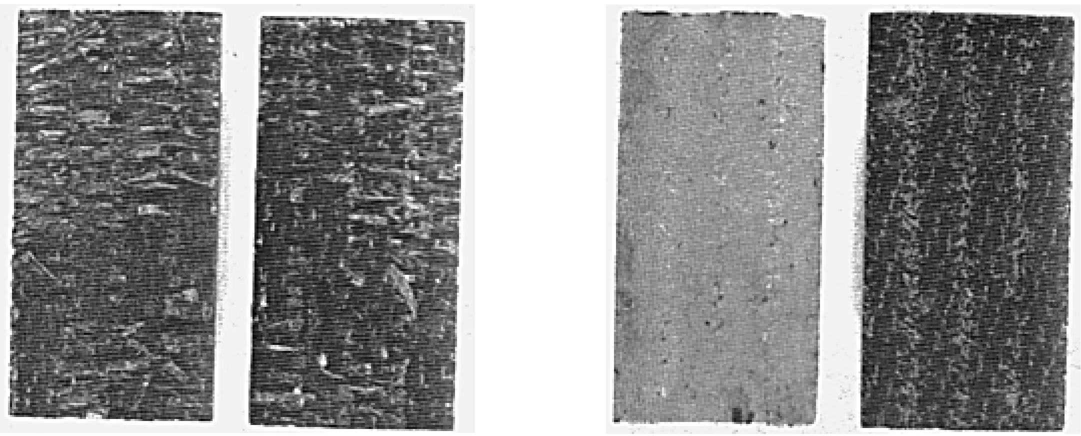

Figure 2. Comparison of a normal ILT failure within the body of the laminate and an adhesive failure which was either a poor bond or a very strong joint indicating very high interlaminar strength in the sample.

As illustrated in Report 1 issued on October 20, densified substrate bearing optimized physical properties generally responds favorably to the SiC coating process. Under these conditions, the coating integrates well with the substrate to give a functional gradient conversion zone in which the SiC phase actually 'blends' into the substrate. This is the desired result expected from the surface conversion process and is most prominent in flat regions. However, the coating-to-substrate conversion zone may be less than optimal in certain panel corners and along curved areas where a distinct boundary between converted and unconverted substrate is relatively easy to see. Coated ILT specimens taken from flat regions exhibiting excellent conversion of the substrate perphery have been tested many times for both ACC and RCC and the failure generally occurs within the body of the substrate laminate. Failures right along the coating interface tend to indicate a poor conversion gradient in that area.

[1]: Images taken from, "ACC Material Characterization Test Specimen Design and Fabrication Preparation of Stitched and Non-Stitched Compression Panels", LTV Report 221RPA0095, NASA-LaRC NAS1-17079, June 1987, R.O. Scott and R.E Lee

Generally, flat 1” X 2” ILT specimens were bonded to both test blocks with the epoxy adhesive and tightly C-clamped for overnight ambient cure. Liberal and uniform squeeze-out along the bond line perimeter was ensured to facilitate a good bonding process. One of the underlying lessons learned from this overall effort was that the bonding interface between the mounting block and sample must be exceptionally flat and the pull axis should directly perpendicular (orthogonal) with the sample plane, otherwise extraneous loading moments were generated which negatively influenced the test results. Considering some of the ILT-type concepts given in one of the recent RCC root cause presentations given in Figure 3 below (“Materials Testing for Root Cause Determination and NDE Correlation”, NASA LaRC, November 5 2007 – Version 5) , one may tend to speculate on the degree of bond line flatness, orthogonality and the number of oblique moments that could possibly be generated.

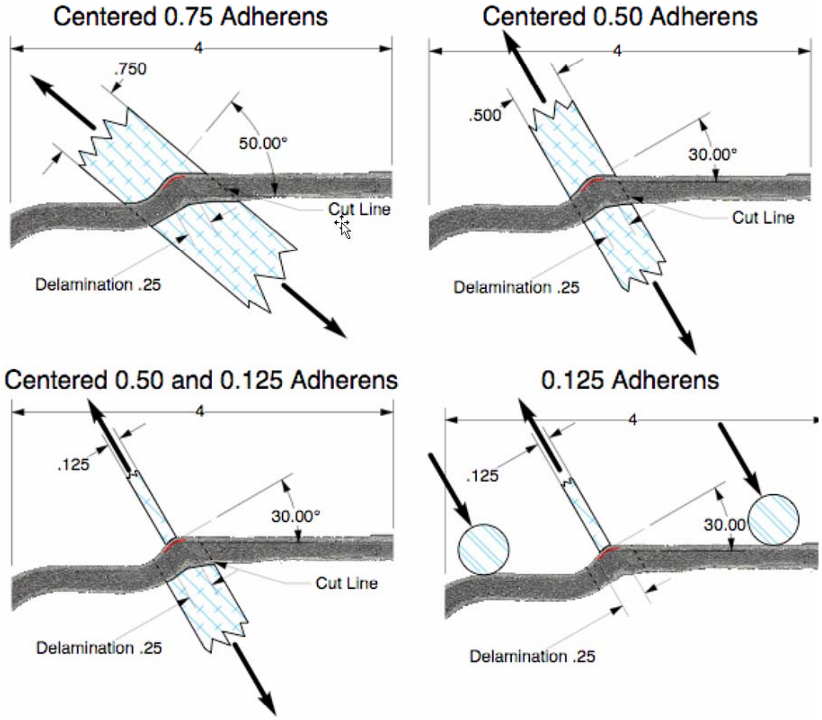

Figure 3. Illustrations of several ILT test configurations proposed by the RCC SiC coating spalling investigation team.

For the two top scenarios, specially machined bonding blocks would be required for each and every test sample because the specific surface contour, morphology and precise OML/IML radius values would be a little different for each joggle section sample (ie... one size will not fit all – the blocks (or rods) will have to be precisely machined to properly mate with each given sample). Since the pull surface for these two configurations contains significant contours (non-flat areas), the effects of diverging moments would probably be exacerbated. Also, since craze cracks are wider in convexed curved regions, adhesive penetration would likely add to the list of ambiguous moments possible. However, these two configurations seem to contain ample bonding surface area, which is a necessity. The bottom two designs also look interesting. However, a very good adhesive would be needed since the contact area is so small. For both of these configurations, one might suspect adhesive failures to dominate most of the results, especially for samples that do not contain any weak planes or delams (which is good of course). The bottom right set-up appears to be essentially a single-sided coating adherence test, which may be more in line with what the RCC Team is seeking rather than a test that loads the entire cross-section of the sample. One might modify the bottom left design so that both upper and lower pull rods are the same diameter. Regardless of which approach is pursued, the requirement for standardization in both flat areas and 'good' joggle radii is mandatory. In all likelihood, many tests would need to be performed on new parts in order to establish a reliable baseline. As the ILT test development history described above indicates, inconsistency and data scatter in just the flat areas of freshly manufactured product was often undesirable and sometimes appalling. With time and perseverance however, these efforts eventually led to a standard ILT test procedure. Ideally, for the current RCC investigation, the task should have been started some time back so that standard (baseline) ILT values were already available and tests could simply be conducted now on questionable parts with a much better assessment in the short run. At this late point in the game, it might cautious not to take the ILT numbers or apparent physical property correlations too seriously when the numbers start rolling in, at least in the beginning.

As the principal ACC laboratory substrate technologist and associate RCC/LESS M&P scientist at LTV during the 1980's (the company's most active time period for RCC production and ACC development), I supervised the LESS/ACC pilot processing line and related R&D activities where I developed, refined and standardized many of the critical physical property and mechanical test methods used for ACC/RCC substrate characterization. Moreover, I adapted and extended these techniques throughout the process sequence... from the as-molded (autoclave cured) condition through each of the subsequent carbon (pyrolyzed) states, all of the intermediate bimatrix (impregnated) states and the final post-coated condition. I conducted and oversaw thousands of tests for the determination of carbon-carbon (composite) bulk density, true density, open porosity, matrix content, matrix density, fiber volume, resin weight gain, pyrolysis weight loss, cumulative & incremental carbon gains, 3 & 4-point flexure, lap shear, double notched shear, short beam shear and ILT strength. One of my primary areas of emphasis was the control (via process modifications), the accurate measurement and consequential effects of substrate density, porosity and matrix content relative to flexural and ILT properties. During this effort, I developed and validated a system of characterization tools which greatly enhanced the ability to estimate and predict composite physical properties as they changed from one state to the next across the entire carbon-carbon manufacturing process. This permitted determination of quantities that were essentially impossible to analytically measure, such as bimatrix content at RCC-2BIM (and ACC-3BIM), carbonized matrix contents at each of the carbon states, and associated matrix volume fraction at RCC-3 (and ACC-4). While it is important to incorporate ILT integrity into the densified composite, perhaps the most important physical property to understand (and manipulate) in order to facilitate optimal SiC conversion of the substrate periphery is the level and nature of pre-coat substrate porosity. The ultimate intent of these modeling tools was to design and execute the initial fabrication molding process and successive densification parameters in efforts to ensure that the properties of the densified substrate were mechanically acceptable and physically receptive to the coating process, rather than tweaking the process from step to step (which was often the norm and may still be).

On a daily basis, substrate porosity was measured using an adapted version of the Archimedes-based ASTM C-20 water boil test for apparent porosity on 1" X 1" X t specimens (where t is the panel thickness). Later on, I developed a special version of this test (modified C-20) based on water impregnation in accordance with the resin densification approach characteristic of ACC and RCC. After the proper technique was refined and established, these methods gave very repeatable values for fluid-accessible porosity and void volume along with the associated composite bulk density and the true (skeletal) density. Incidentally, I was given charge of the Quantachrome Mercury Porosimetry testing system when it came in house, and after many trials and correlation attempts, it was concluded that mercury porosimetry was inadequate for carbon-carbon (actually, for composites and ceramics in general) because it irreversibly damages the sample, destroying the very property under investigation. Other workers later confirmed these results. The water boil and impregnation techniques continued to be the primary methods for porosity measurement. While these density/porosity tests also derive the composite bulk density (and composite true density), much of the time, reported bulk densities were actually determined geometrically by weights and measures. Flexure bars were typically 0.8" X 6" and could sometimes be used for subsequent porosity/density testing, resin content or microstructural analysis. After multiple trials, short beam shear samples of 1.5" X 0.5" X t size gave good results but did not seem to reveal much quantitatively from panel to panel (the method should have probably been developed further). Lap shear samples were specially fabricated during the initial lay-up of a reserved test panel and this method produced the best results for determination of interlaminar shear strength, but required a dedicated test panel.

Over the course of several years, perhaps a couple of hundred thousand data points were manually entered into my TI calculator(s) (this was before PC's were prevalent on the desktop). Data reduction, analysis and correlations between physical properties and process parameters were carried out using ACC and RCC buttons, bars, squares, disks, blades, tee-sections, angled segments, trimmed control panels and full sized test articles. Most of the data and information I have access to at this point in time is related to uncoated ACC substrate. However, all the analysis methods and characterization tools developed during this period were repeatedly proven to work extremely well for both ACC and RCC material systems. Now from the coating perspective, relationships between coating-to-substrate compositional gradients, carbon weight gain (or matrix content) and the final (densified) substrate porosity are mandatory in order to ensure proper compatibility between the coating phase and the substrate. On the substrate side, composite densities, mechanical attributes (especially ILT strength) and fiber volume seem to be the controlling factors defining mechanically optimal substrate. Many of my studies demonstrated that unique relationships can be derived between composite densities, matrix fractions, open porosity, flexural and ILT strength as well as most of the processing parameters leading up to any point of interest upstream or downstream. As one would expect, reduced averages from larger data pools usually produced better results than those that were attempted with the raw data itself, which often gives obscure scatter plots. And sometimes, data deemed most suitable for correlations consisted of averages of averages. As a simplified example, consider some of the pre-coat substrate data generated during one of the NASA ACC projects undertaken during the 1980's as depicted in Table 1 below.

Table 1. Final ACC substrate test data taken from "NASA Langley Impact Panels, Substrate Report, Randy Lee, 11/85" demonstrating apparent physical property dependence on the number of plies in a laminate.

ACC-4 Mechanical / Physical Test Data

Panel ID (ply count)	Bulk Density (g/cm^3)	Per Ply Thickness (mil)	ILT Strength (PSI)	Flexure Strength (KSI)	Open Porosity (%)	True Density (g/cm^3)
6A	1.65	11.0	average of 3	average of 3	7.2	1.78
6B	1.66	10.8	taken from	taken from	7.8	1.80
6C	1.65	10.8	control panel	control panel	7.2	1.78
6D	1.66	10.7	872	39.4	6.7	1.78
6 ply	<1.66>	<10.8>	<872>	<39.4>	<7.2>	<1.79>
12A	1.67	10.6	average of 3	average of 3	6.4	1.78
12B	1.67	10.7	taken from	taken from	6.3	1.78
12C	1.66	10.6	control panel	control panel	6.2	1.77
12D	1.67	10.6	900	43.6	6.8	1.79
12 ply	<1.67>	<10.6>	<900>	<43.6>	<6.4>	<1.78>
18A	1.67	10.5	average of 3	average of 3	5.6	1.77
18B	1.68	10.5	taken from	taken from	5.9	1.79
18C	1.68	10.4	control panel	control panel	5.9	1.79
18D	1.68	10.4	860	38.8	6.7	1.80
18 ply	<1.68>	<10.5>	<860>	<38.8>	<6.0>	<1.79>

R.C. Lee
11/85

In this task, flat panels of three different thickness categories (6, 12 and 18 plies) were fabricated using 8 harness PAN fabric in 0°–90° cross-ply configuration and phenolic matrix densification throughout. Physical/mechanical characterization was performed in the as-molded state and at the end of four densification cycles. I personally conducted and oversaw the design, fabrication and characterization of these test articles from the prepreg state to fully densified ACC-4 prior to coating. Unlike some of the other methodologies in practice at the time, I drove the extra mile to ensure precise processing and superior data gathering technique for each and every LESS-related task under my responsibility. Throughout all my studies, physical property relationships and state-to-state changes that could be mapped out using asymptotic-type functions seem to be a recurring theme. This task (as well as several others) gave strong indications that, under standard processing conditions, some of the physical properties bear direct relationships with the number of plies comprising the laminate. From Table 1, consider the bulk (geometrical) density and open porosity averages as plotted and functionally fitted in Figure 4 below.

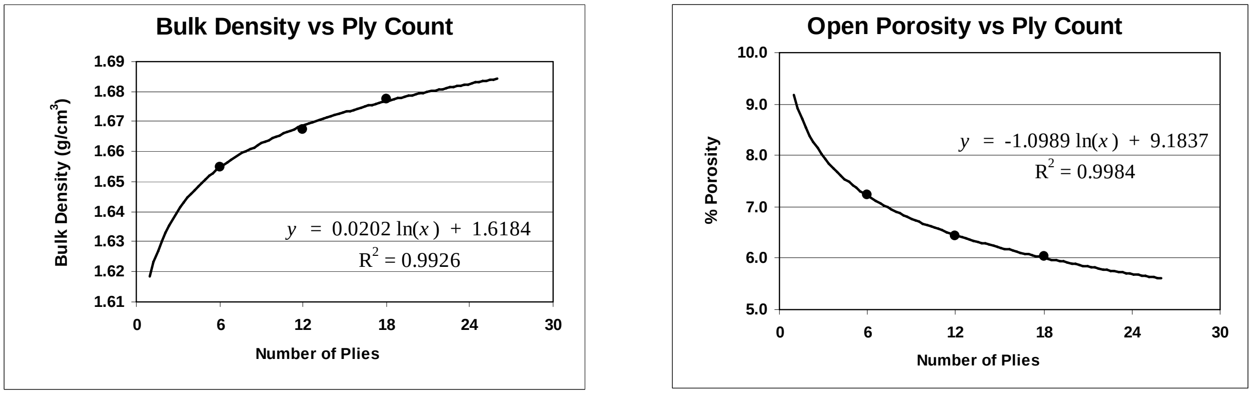

Figure 4. Plots with curve fits of average bulk density and average porosity for each of the three thicknesses (number of plies) given in Table 1.

Typical engineering convention might be to fit these points to linear or polynomial functions and be done with it. However, attempts to explore the scientific extremes often lead to interesting insights regarding the behavior of certain properties near their theoretical minimum and maximum regions. Personal experiences in this area have taught that many of the physical properties asymptotically approach either one or both of their extreme values when plotted against one another, across a time line or through a step-by-step process (but not always). Even though the baseline parameter is incremental (or discrete), continuous functions can be utilized, keeping in mind that the x-axis is often defined by integers. For this particular data, logarithmic representations seem to provide adequate fits for these properties in the range of values tabulated while considering the possible extremities. Here, the bulk density appears to approach a minimum of 1.618 g/cm^3 at one ply thickness and vanishes after that. On the other end, bulk density very slowly approaches the true composite density (~ 1.8g/cm^3) at almost 5000 plies while the porosity approaches zero. These functions may not be flawless in all respects, but for the moment, they do tend to address both the practical and theoretical ranges of interest.

So why did the bulk density go up and the porosity go down with laminate thickness in this study? Examination of the as-molded data (available but not given here) reveals these exact same trends of increasing density, decreasing porosity and decreasing per-ply thickness with ply count, and all sample sets were cured in the same autoclave run under the same lay-up and bagging conditions. Thus, the factors causing this behavior were established during the initial autoclave fabrication stage and not during the densification process. Note also, that the decreasing per-ply thickness given in Table 1 supports the trend of increased compactness with increasing ply count. Consider the fact that as laminates cure, the majority of the resin out-flow is across the plies. Perhaps the thicker laminates experienced more cross-sectional bleed-out resulting in more ply-to-ply compaction with less interlaminar porosity, along with greater fiber volume and thus, higher composite density. Since the fiber density is substantially greater than that of the resin, increased compaction with decreased resin content could conceivably increase the composite bulk density while resulting in less interlaminar binding resin between plies . . . and lower ILT with increased thickness (of course, resin distribution become progressively worse with increasing thickness). Perhaps this effect could be confirmed from the weight loss upon autoclave cure and as-molded resin content, parameters that were normally recorded for all articles (when feasible) but were not available for this report.

Now the true composite density (skeletal or impervious density) refers to the non-porous portion of the substrate (i.e... the fiber and matrix only) and approaches the bulk density when the pore volume approaches zero. If W and V are the actual panel weight and volume respectively, and p, v_f, v_m and v_p are the porosity volume fraction, actual volume of fiber, actual volume of matrix and actual volume of pores (and voids) respectively, then the true density can be given as [1]...

$$\rho_t = \frac{W}{v_f + v_m} = \frac{W}{V - v_p}$$

$$\rho_t = \rho_b \left(1 - p\right)^{-1} \qquad (1)$$

As seen from this relation, the impervious composite density is a calculated quantity but is a direct function of the measured values for bulk density and open porosity. Consider now, from Table 1, the possible relationship between the average ILT values for each ply level and the corresponding true density averages. A plot and functional fit using the expected extremes [2] and a fiber density of ρ_f = 1.92 g/cm^3 along with a localized fit using just the local data are given in Figure 5.

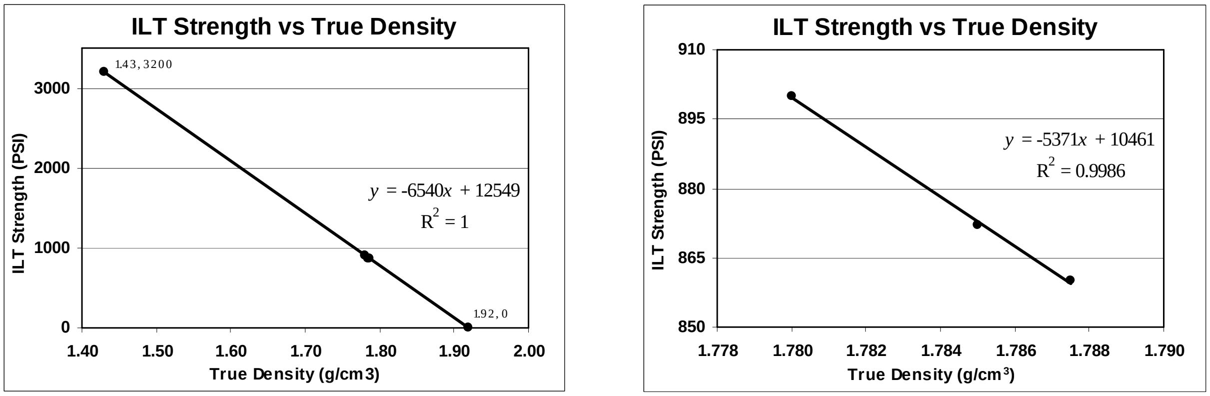

Figure 5. Linear curve fits for average ILT strengths and true densities for each of the three thicknesses (number of plies) given in Table 1.

[1]: All expressions and derivations presented throughout this paper are excerpts from a more comprehensive model that started with the study, "Relationships in Carbon-Carbon Substrate Processing", Randy Lee, LTV Aerospace & Defense Co., LESS Program, 1986. Further refinement and verification of these tools continued with subsequent studies and publications.

[2] Numerous tests have been perfomed (personally) in efforts to physically and mechanically characterize the properties of the specific phenolic resin used during this activity (a Borden resole of ~70% solids, circa 1985). For these studies, samples of the phenolic resin cured at 325°F under 90psi (standard processing conditions) were determined to have an average impervious density of 1.26 g/cm^3. Its tensile strength was around 4000–4500psi (4300psi is arbitrarily used throughout this report). When cured phenolic resin samples were pyrolized (carbonized) to 1500°F, the average char yield was found to be right around 56%. Carbonized phenolic resin (glassy carbon) was determined to have an average impervious density of 1.43 g/cm^3 after pyrolysis, and a tensile strength of 3000-3500 psi (3200 is used here). The density of carbonized PAN fibers utilized during this period was determined (by myself and Fiberite) to range from 1.91 g/cm^3 to 1.96 g/cm^3.

Perhaps the most important question to ask here is why ply-to-ply (interlaminar) strength goes down as the composite density increases. This can be justified by considering a few relevant pieces of information. Recall that ILT strength is essentially a measure of fiber-to-matrix adhesion, so that as the fraction of matrix decreases (and the fiber fraction increases), the system density increases and theoretically approaches the fiber density. At this extreme point, the matrix vanishes and ILT goes to zero. On the other side of the function, as the fraction of fiber decreases and matrix fraction increases, both the system density and ILT strength approach those of the matrix. In the left hand graph, the impervious density of carbonized phenolic resin has been measured [1] at 1.43g/cm^3, (both phenolic and furfurylol resins form vitreous/glassy amorphous carbon upon carbonization) and the impervious density of carbonized PAN fiber is taken as 1.92 g/cm^3. Also, an ultimate tensile strength of 3200psi is utilized here for carbonized phenolic resin (it is worth noting here that glassy carbon matrices derived from phenolic polymers are quite unique, they are strong, non-graphitizable hard carbons possessing an appreciable degree of oxidation resistance – unlike most other carbon forms). In these characterizations, simple linear fits are deemed appropriate for effectively covering both the relevant extremities and local points of interest.

A possible implication here might be that precise ASTM C-20 (density/porosity) measurements of a composite (or more importantly, a specific region of interest within the composite) might provide correlation information regarding local ILT properties and could even be indicative of the presence of undesirable weak planes within the laminate network. The apparent relationship between ILT and true density has not always been as pronounce for every project undertaken as it was with this one which allowed direct comparison of three different ply categories. As will be shown shortly, ILT bears a more consistent relationship with the matrix content.

As another example, consider some of the information gathered during fabrication and characterization of angled panels (T-sections) generated as part of a larger project investigating ACC post-buckling theory out of LaRC [2]. The diagrams and data given in Table 2 below indicate the specific tests and location of specimens evaluated as one of these segments was subjected to as-molded physical/mechanical testing and its companion segment was densified through four carbon-carbon cycles to the pre-coat ACC-4 state.

NASA LaRC Task III Single Stem 6-Ply Compression Panels

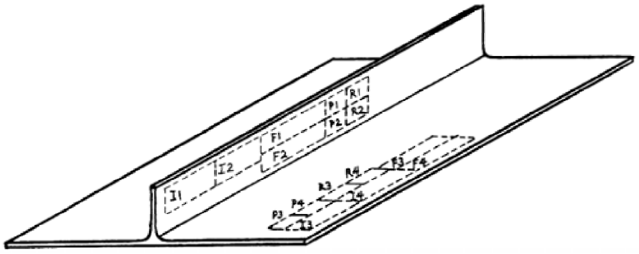

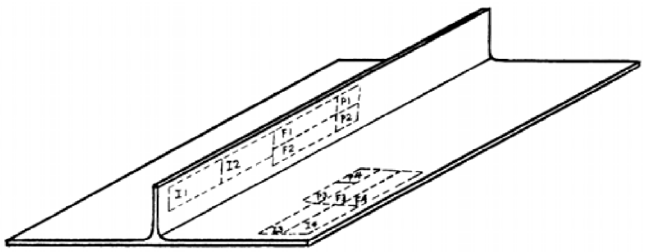

As-Cured Physical/Mechanical Test Data

Specimen	4-Point Flexural			ILT	ASTM C-20		Resin
ID	Thickness 6 Ply Panels) (mil/ply)	Strength (KSI)	Modulus (MSI)	Strength (PSI)	Bulk Density (g/cm^3)	Apparent Porosity (%)	Content (Nitric Acid) (%)
F1	11.5	45.2	18.4				
F2	11.7	46.7	18.6				
F3	11.7	41.7	18.1				
F4	11.5	46.5	18.1				
I1				1336			
I2				1286			
I3				1169			
I4				1142			
P1					1.60	5.77	
P2					1.60	5.67	
P3					1.57	6.06	
P4					1.59	6.18	
R1							30.5
R2							28.7
R3							28.5
R4							27.4
$\langle x \rangle$ =	11.6	45.0	18.3	1233	1.59	5.92	28.8
% σ =	1%	5%	1%	8%	1%	4%	4%

ACC-4 Physical/Mechanical Test Data

Specimen	4-Point Flexural			ILT	ASTM C-20	
ID	Thickness 6 Ply Panels) (mil/ply)	Strength (KSI)	Modulus (MSI)	Strength (PSI)	Bulk Density (g/cm^3)	Apparent Porosity (%)
F1	11.3	44.7	17.4			
F2	11.2	43.4	16.8			
F3	11.3	39.7	17.4			
F4	11.3	41.8	16.6			
I1				909		
I2				862		
I3				858		
I4				840		
P1					1.62	9.27
P2					1.62	8.96
P3					1.66	8.37
P4					1.65	9.00
$\langle x \rangle$ =	11.3	42.4	17.1	867	1.64	8.90
% σ =	0%	5%	2%	3%	1%	4%

R.Lee
1/87

Table 2. As-molded and fully densified ACC-4 charaterization data and selected specimen locations for 6-ply stemmed compression panels

---

[1] See page 6 footnote 2.

[2]: Taken from, "ACC Single Stem Compression Segments, Substrate Report", NASA LaRC, Randy Lee, LTV Aerospace & Defense, LESS Program, 1987. Processing, analysis and illustrations by Randy Lee.

The articles in this series of panels were each fabricated using typical 0°–90° cross-ply configurations and matching male-female tooling with strategically placed filler strips and bundle strands along the radius (T angle gap). Each 6 ply lay-up utilized two plies of bleeder canvas (tapered into the radius areas), barrier film and three plies of breather material, and the entire tooling/lay-up assembly was envelope bagged for cure. The standard ACC autoclave cycle was also used which consisted of 2°–3°F/min heating ramps with 1 hour holds at 180° and 325°, 10 psi pressure and full vacuum throughout. I personally conducted the planning, hands-on fabrication, physical testing, data analysis and final laboratory report. Due to the matched aluminum tooling components and hand crafted lay-up techniques, there was no evidence of resin rich or resin starved regions along either the OML or IML radius surfaces. Flexural, ILT and C-20 tests were conducted in both the as-molded state and at ACC-4, except resin content analysis was performed in the as-cured state (via ASTM nitric acid digestion). Note that two resin content samples were evaluated along the stemmed section and two were taken from the main panel area, while in the fully densified segment, ILT specimens were extracted in similar regional proximities. Also, make reference to Table IA in Appendix I which contains the associated densification data for this series of panels as they were processed from the ACC-0 pyrolyzed (carbon) state through each of the intermediate carbon states and subsequent impregnation/cured (bimatrix) states to the ACC-4 fully densified (pre-coat) carbon state.

Meaningful correlations for more advanced studies are often difficult to draw using raw data and may be more revealing when reduced data averages are available similar to the values given below each of the columns in Table 2 and Table IA. However, before examining the fully densified state, in the as-molded condition, Table 2 does seem to indicate a slight dependence of ILT strength on laminate resin content (as-molded matrix content). If we consider the theoretical maximum strength of a composite consisting of cured phenolic resin matrix to be ~ 4300 psi [1] at 100% resin content and 0 psi at the other end, corresponding to zero resin content, then both local and comprehensive data fits seem to coincide fairly well overall as shown in Figure 6 below.

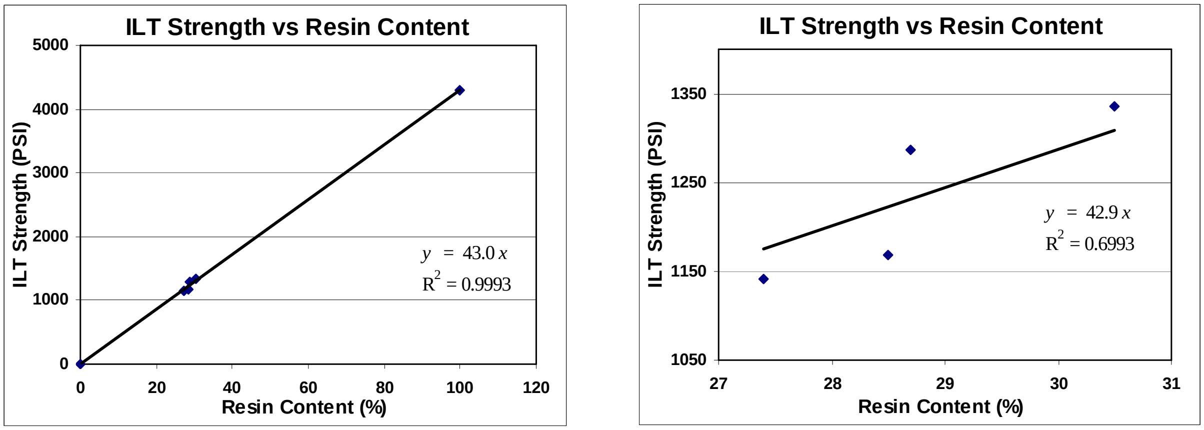

Figure 6. Curve fit analysis of measured ILT strengths and resin content values for the as-cured panel samples defined in Table 2

In support of some of the results previously shown, this strongly indicates that *ILT strength is a matrix-dominated property* regardless of whether the matrix is comprised of organic thermoset polymer or its carbonized pyrolytic form as deposited within the RCC/ACC porosity networks. It has been shown that the need to characterize the matrix phase (matrix content, matrix volume) prior to coating operations (ACC-4, RCC-3) is quite crucial in understanding the product's coating feasibility as well as its ILT properties. From a measurement perspective, degradation of the fibrous phase is negligible in hot mineral acids while crosslinked organic polymer matricies are easily digested in hot nitric or sulfuric acids . . . but glassy carbons are completely inert to acid degradation. Consequently, physical measurements for matrix content have been impossible to obtain for both RCC and ACC substrates at any of the carbon states. However, after considerable number crunching and data analysis, a method was developed that turned out to quite helpful in facilitating estimates for carbonized matrix content (and volume) along with several other of the more critical material properties. A number of 'densification studies' were conducted in which I precisely measured all the physical and mechanical properties of the substrate at each of the processing states, reduced the data and established a series of property-process correlations. The now famous 'rule of mixtures' approach provided a good starting point and has proven to work extremely well in these studies. Consider the following analytical scenario which was developed during work on ACC material and was subsequently applied in numerous projects [2]. It has been proven to be equally valid for RCC articles undergoing furfuryl alcohol densification to the RCC-3 state (and beyond).

[1] See page 6 footnote 2.

[2] See page 6 footnote 1.

At any point during the fabrication (or lifetime) of a composite substrate, the bulk density can be defined as the sum of the products of each constituent density and its respective volume fraction...

$$\rho_b = \frac{w_f + w_m}{V} = \frac{\rho_f v_f + \rho_m v_m}{V} = f_v \rho_f + m_v \rho_m$$

where w_f, w_m, v_f and v_m are the actual weights and volumes of the fiber and matrix phases comprising the panel, article or sample which has an actual weight and volume of W and V. Accordingly, ρ_f and ρ_m are the impervious fiber and matrix densities, and f_w, m_w, f_v, m_v and p are the fiber and matrix weight fractions, along with the fiber, matrix and porosity volume fractions respectively.

Here, we make use of the fact that both the sum of fractions by weight and the sum of fractions by volume are always unity. Respectively...

$$f_w + m_w = 1 \qquad \text{and} \qquad f_v + m_v + p = 1$$

Also, fiber and matrix volume fractions can be expressed in terms of their respective weight fractions. Since

$$\rho_f = \frac{w_f}{v_f} = \frac{f_w W}{f_v V} = \frac{f_w}{f_v}\rho_b \,, \qquad \text{then} \qquad f_v = f_w \frac{\rho_b}{\rho_f} = \left(1 - m_w\right)\frac{\rho_b}{\rho_f} \,.$$

$$\text{Likewise...} \qquad m_v = m_w \frac{\rho_b}{\rho_m}$$

With inclusion of the porosity fraction, the bulk density can be written in terms of component weight fractions...

$$\rho_b = \frac{W}{v_f + v_m + v_p} = \left(f_w \rho_f^{-1} + m_w \rho_{\mathrm{m}}^{-1} \right)^{-1} \left(1 - p\right) \tag{2}$$

While bulk density is defined by constituent volume fractions, the true composite density (defined earlier in Eq(1)) is a function of the weight fractions and represents the impervious density of the composite...

$$\rho_t = \left(f_w \rho_f^{-1} + m_w \rho_{\mathrm{m}}^{-1} \right)^{-1} = \rho_b \left(1 - p\right)^{-1}$$

Rearrangement of Eq(2) gives an expression for estimating the porosity from the fiber density, matrix density and matrix content (in the as-molded state, this would pertain to the cured resin density and resin content)...

$$p = 1 - \rho_b \left[\left(1 - m_w\right) \rho_f^{-1} + m_w \rho_m^{-1} \right]$$

For example, using an average resin content and bulk density from Table 2 (m_w = 28.8% and ρ_b = 1.59 g/cm^3), along with a fiber density [1] ρ_f = 1.95 g/cm^3, and cured resin density ρ_f = 1.26 g/cm^3, the estimated porosity for the as-molded article given in Table 2 is a comparable p = 5.6%.

After the initial autoclave molding process is complete, the densification phase commences where the panel undergoes several cycles of pyrolysis and resin impregnation/cure (it is weighed before and after each step). The *positive* weight loss η_l, due to pyrolysis of an article in a cured or bimatrix state to the next corresponding carbon state, and the weight gain η_g, that occurs when an article in a carbon state is impregnated with resin both result in changes within the matrix exclusively and can be represented by...

$$\eta_{li} = \frac{W_{(i-1)B} - W_i}{W_{(i-1)B}} = \Delta m_{w(i-1)B \to i} \qquad \text{and} \qquad \eta_{gi} = \frac{W_{iB} - W_i}{W_i} = \Delta m_{wi \to iB}$$

where each step in the process can be recognized by subscripts denoting one of the carbon states, $i =$ 0, 1, 2, 3,... or one of the bimatrix states [2], $i =$ 0B, 1B, 2B,...

---

[1] See page 6 footnote 2.

[2] Bimatrix (B or BIM) pertains to substrate in which the matrix consists of two distinct phases. In the case of RCC and ACC composites, varying portions of cured polymer resin and previously deposited charred resin simultaneously comprize the matrix at any of the impregnated states.

Consider the first pyrolysis which takes the panel from the as-molded condition to the first carbon state (-0) in which the substrate weight changes by $W_A = W_0 \left(1 - \eta_{l0}\right)^{-1}$ . . .

$$\eta_{l0} \; = \; \frac{W_A - W_0}{W_A} \; = \; \frac{\left(w_{mA} - w_{m0}\right)}{W_A} \; = \; m_{wA} - \frac{y w_{mA}}{W_A}$$

$$\eta_{l0} = m_{wA}\left(1 - y\right)$$

where y is the char yield of the resin matrix [1].

Now the matrix weight fraction at the first carbon state, ACC-0 (or RCC-0) becomes...

$$m_{w0} = 1 - \frac{w_f}{W_0} = 1 - \frac{w_f}{W_A\left(1 - \eta_{l0}\right)} = 1 - \frac{f_{wA}}{1 - \eta_{l0}}$$

$$m_{w0} = 1 - \left(1 - m_{mA}\right)\left(1 - \eta_{l0}\right)^{-1} \tag{3}$$

$$m_{w0} = 1 - \left(1 - m_{mA}\right)\left[1 - m_{wA}\left(1 - y\right)\right]^{-1} \tag{4}$$

Using the averages $m_{wA} =$ 28.8% from Table 2 and $\eta_{l0} =$ 11.6% from Table IIA, the estimated average matrix content for the four as-molded samples given in Table 2 after pyrolysis to the first carbon state comes out to $m_{w0} =$ 19.5% when Eq(3) is used, and gives $m_{w0} =$ 18.5% when Eq(4) is utilized along with $y =$ 56%.

After the first impregnation and cure, the bimatrix weight fraction becomes...

$$m_{w0B} = 1 - \left(1 - m_{mA}\right)\left(1 - \eta_{l0}\right)^{-1}\left(1 + \eta_{g0}\right)^{-1}$$

and in general (after each densification cycle) ...

$$m_{wi} = 1 - \left(1 - m_{w0}\right)\prod_{0}^{i}\left(1 - \eta_{l1}\right)^{-1}\left(1 + \eta_{g(i-1)}\right)^{-1}$$

or ... (5)

$$m_{wi} = 1 - \left(1 - m_{wA}\right)\prod_{0}^{i}\left(1 - \eta_{li}\right)^{-1}\prod_{1}^{i}\left(1 + \eta_{g(i-1)}\right)^{-1}$$

With each densification cycle, pyrolyzed resin (glassy carbon) is deposited within the porosity of the substrate. Incremental carbon weight gain due to the first cycle (that is, going from carbon state $0 \to 1$), can be estimated from panel weigh gains at each carbon state and is a measure of the matrix change from one carbon state to the next carbon state, that is... $\eta_{c0\to1} \; = \; \left(W_1 - W_0\right)W_0^{-1} \; = \; \Delta m_{w0\to1}$. It has been shown [2] that cumulative carbon gains can be written in terms of incremental carbon gains...

$$\eta_{c0\to i} = \eta_{c0\to1} + \sum_{2}^{i}\eta_{c(i-1)\to i}\prod_{2}^{i}\left(1 + \eta_{g(i-2)}\right)\left(1 - \eta_{l(i-1)}\right)$$

Historically, carbonized matrix fractions at any of the carbon states have been physically impossible to measure, but pre-coat (ACC-4) matrix content values for each of the four specimens given in Table 2 can be reasonably estimated with the following approach. Using the average resin content value, m_{wA} = 28.8% from Table 2 along with Eq(5) and the initial pyrolysis weight loss η_{l0} for each of the seven panels given in Table IA (Appendix I), the first carbon matrix weight fraction m_{w0} for each panel can be estimated. Now, using the subsequent weight gains and losses, matrix fractions can be determined for all seven panels at each carbon state up to ACC-4, and the averages for all seven panels can be plotted and curve fitted, as shown in Figure 7 below.

---

[1] See page 6 footnote 2.

[2] See page 6 footnote 1.

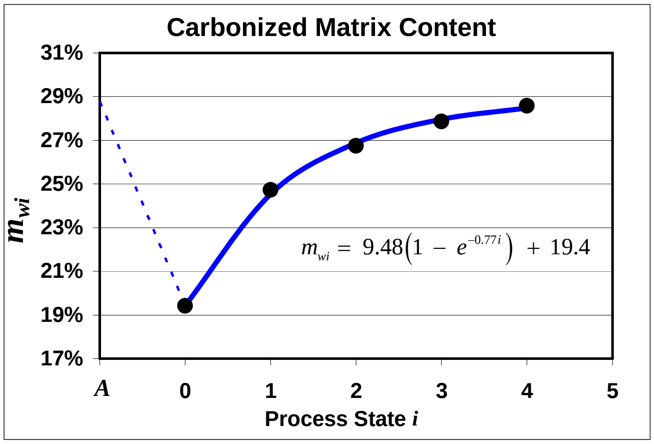

Figure 7. Plotted average matrix content values for the 7 panels in Table IIA along with the corresponding model curve fit.

Here, $m_{w0} = 19.4\%$ and approaches a maximum value of $9.48 + 19.4 = 28.9\%$ after an infinite number of densification cycles. It has been repeatedly shown [1] that substrate matrix content, bulk density, carbon weight gain, ILT strength and flexure strength all follow this same functional trend, asymptotically approaching a theoretical maximum across the process, while decreasing properties, such as open porosity and fiber content, approach a specific minimum. In general, increasing properties and decreasing properties can be represented respectively by...

$$P_i = A\left(1 - e^{-ki}\right) + P_0 \quad \text{and} \quad P_0 = Ae^{-ki} + P_0$$

Now, the functional fit given in Figure 7 can serve as a 'model' for estimation of the matrix content values for each of the four specimens given in Table 2, first by computing m_{w0} for each specimen using Eq(4) and then using the model to determine all of the m_{wi} values for each of the four specimens across the process (each generating a curve similar to that in Figure 7). Of particular interest here are the final ACC-4 pre-coat values which are plotted against the raw ACC-4 ILT strengths given in Table 2 and linearly fitted as shown in Figure 8.

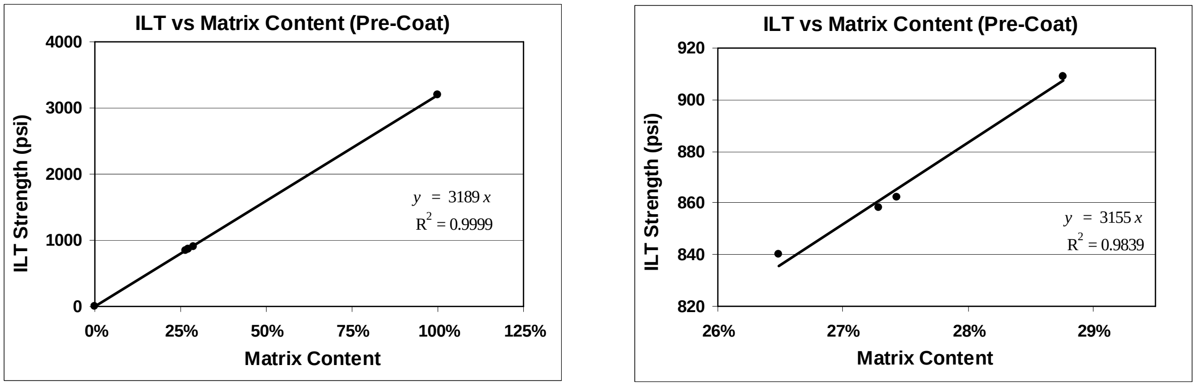

Figure 8. Curve fit analysis of measured ILT strengths and estimated matrix content for the pre-coat panel samples defined in Table 2

Using again, 4300psi as the tensile strength of the carbonized substrate matrix, the local and comprehensive functional fits almost coincide. Although the trend here reflects a distinct relationship between ILT and matrix content, there is surely a coincidence factor involved since the initial resin content samples and densified ILT specimens were not in the exact locations. Nevertheless, this result lends further credibility to the apparent fact that ILT strength is directly proportional to the matrix content, which of course, should not be surprising. Matrix-dominated ILT is likely an inherent property in all laminated composite systems, industry wide. Of interest here is the indication that this dependency holds true even for carbonized matrix systems such as those in RCC and ACC. Although carbonized polymers may not provide quite the binding strength as their organic thermoset counterparts, they are measurably superior to carbon matrix systems formed by other means currently utilized throughout the industry (such as CVI/CVD) in terms of both binding strength and oxidation protection.

---

[1] See page 6 footnote 2.

Indications are that Figure 8 depicts the matrix content of the substrate before *and after* it has undergone the conversion coating process, but it only represents the ILT strengths prior to coating. While substrate mechanical values are substantially degraded as a result of the 3000° SiC surface conversion process, previous testing and experiences have indicated that most of the changes in the other substrate properties are almost insignificant, including substrate densities, porosity, matrix content, fiber volume and per-ply thickness (minuscule changes may include slight widening of the pores and immeasurable density compactness with trace volatile releases). After being subjected to the final coating operation however, measured mechanical properties of the substrate are degraded drastically, including flexural, short beam shear and most importantly, ILT. Post-coat testing has confirmed these effects on every occasion (no post-coat data is available at this time, unfortunately). In the majority of tests, ILT specimens of well coated substrate typically failed within the substrate laminate, occasionally on the substrate side of the conversion zone, and never in the coating body itself. This implies that for optimally coated substrate, the coating-to-substrate bonding interface (a gradient bonding zone rather than a discernable interface) should be stronger that the (weakened) substrate interlaminar ply-to-ply strength.

So why does the coating process degrade ILT or, why is the substrate ILT so greatly reduced when subjected to the coating process? While post-coated RCC specimens generally indicated an ILT loss in the 30-50% range compared to bare RCC-3 samples, ACC-4 ILT values typically dropped a disheartening 50-70% after substrate coating operations. These relative differences can be explained by the presence of much greater nesting effects between plies in rayon-based RCC laminates . . . along with RCC's higher matrix content. Comparatively, PAN-based ACC exhibits very little interlaminar nesting, and carbonized matrix contents are 10-15 points lower that of RCC. In general however, it is likely that the high coating temperature begins to degrade matrix-to-fiber interactions by destroying chemical bonding links between matrix and fiber atoms (i.e... fiber surface functional groups). After all, substrates never see higher than about 1500°F during densification processing while the coating regime takes the substrate up to ~ 3000°. These effects should be investigated further.

Possible Recommendations and Closing Comments

If porosity measurements are tasked by the team, the following suggestions might be considered. Rather than evaluating samples across the entire thickness, if might be more informative to extract independent porosity/density specimens from the extreme OML and IML regions of the *substrate* volume. Specimens might be machined out of these areas as indicated below that are about 0.1" in height X 0.3" wide X .5" deep (into the page) with two specimens in tandem (1" total into the page, i.e... specimen 1 is shown and specimen 2 is behind it).

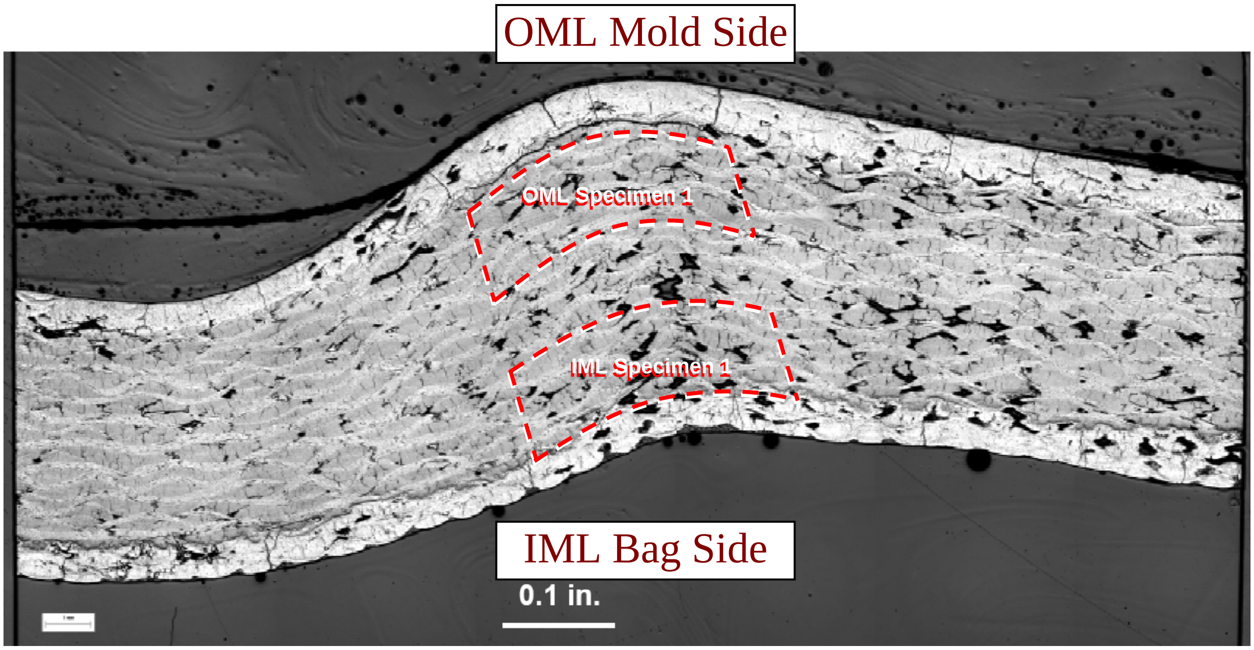

The OML specimens represent the higher density, lower porosity areas of the radius cross-section which is under in-plane tension while the IML specimens would be the lower density, higher porosity region under in-plane compressional forces. Keep in mind that only one sample per area is a shot in the dark, two samples (as suggested) are better, while three to five samples are preferred (if it were possible). Porosity/density measurements via ASTM C-20 or He picnometry might be the recommended approaches. As with ILT test results, limited porosity/density data can be not only be wrong, it can sometimes be grossly misleading. It should be understood that measured values of 'open' porosity and void space within a sample or region are actually a function of the technique used to measure them. While the total porosity of any system is the sum of the open and closed porosity fractions, in some cases, it may be difficult to precisely quantify that portion which happens to be closed and sealed off from the medium trying to gain access to it. Ideally, a comprehensive equation should include the total theoretical porosity, regardless of the fluids or gases used in the process, but this may not always be possible or practical. Incidentally, I developed a correlation between measured C-20 porosity values and raw ultrasonic attenuation levels (U/S scans were typical for most ACC and RCC panels fabricated). In this work, a relationship was established and confirmed for both low and high levels of porosity (overall), but the activity was cut short due to extraneous factors. A precise, regional correlation between measured porosity values and any NDE technique would be beneficial to the entire composites industry. IR Thermography has recently proven itself to be quite an innovative NDE tool for indicating interlaminar gaps, coating separations and suspect high void areas within the RCC periphery. There is a possibility however, that this method might not reveal a whole lot about the failure mechanism if the roots begin far upstream, like in the fabrication stage. In general, no NDE tool currently available can actually detect weak planes or residual stresses, they can only indicate delams or separations after a physical gap has already been initiated. There is nothing consistent about delamination events. Especially under cycling and fatigue conditions, a weak plane may gradually progress and slowly delaminate, but other times, it may hardly move at all and then suddenly snap or increase markedly.

The ‘convolutions’ discussed in several of the recent RCC presentations are actually buckled fabric layers under in-plane compression that tend to ‘bunch up’ (or buckle) near the IML side of the radius during the lay-up and molding processes. See RCC Report 1. The fabric tends to buckle in the IML region rather than in the OML side but the effect can sometimes carry into the cross-section toward the OML during the autoclave curing process. The mechanics behind this phenomena can be explained as follows. During the lay-up process, the fabric layers are stretched across the wider OML surface one by one as the thickness is gradually built up. At about 6 or 8 plies, the layers often begin to (slightly) buckle in on themselves (slightly). This effect gets progressively worse as the lay-up continues and the fabric layers are continually forced into a narrowing IML radius (classical thick laminate physics inside a radius). This effect has always been common in troublesome radii of both RCC and ACC contoured articles (the condition is latent in almost all laminated composites throughout the industry). Over the years, refinements in RCC prepreg hand lay-up techniques, bleeder/breather/bagging modifications and custom tooling aids have significantly reduced this problem from what it once was. While I am aware that certain regions in some of the RCC panels utilize filler strips, I cannot recall precisely if these particular joggle regions did. To my recollection, they did not, but that could have changed over the years. In any event, if filler strips are present, they would not be the cause of the convolutions, the IML buckling/bunching effect is, as previously described. Also, note that this buckling/bunching effect originates from the IML side, opposite to the OML which is under radial tension where the delams are occurring. Its physical role in the OML delams is probably insignificant. On the IML side of the radius however, these buckled fabric layers can become a major weak point in the structure and could facilitate a failure in the laminate originating from the IML side, particularly if loaded in a manner that forces the radius section open or in on itself. Another test we sometimes did for angled sections was to measure the load required to fail the sample by pushing the radius open or shut... a corner flexure test. Not sure of the interest level or how valuable this type of non-standard test might be for the current investigation, but given the apparent joggle region property distribution and associated IML buckled condition, these samples would likely fail much of the time on the IML side (first) and indicate little about conditions on the OML side or the root cause under investigation.

After DTA implementation, TEOS undoubtedly penetrates deeper into the substrate. However, recall that during the densification phase, low viscosity furfuryl alcohol resin is forced into the substrate unhindered (bare substrate, no pores blocked by the coating) using vacuum *and pressure* in three successive cycles. Closed pores inaccessible to three separate cycles of the more aggressive furfurylol impregnation should be more difficult to infiltrate during TEOS vacuum-only impregnation. Prior to coating operations, the RCC-3 substrate porosity may run 10-15% and the coating temperatures may slightly open up the existing pores somewhat, but no new porosity is created within the substrate body during the coating process. The autoclave fabrication process and first pyrolysis establish the primative interconnecting porosity network within the substrate and densification successively deposits carbonized polymer along the walls of these tunnels as the matrix is built up. At RCC-3, most of the smaller surface pores are filled during the SiC conversion process and others are blocked off by the coating itself (SiC occupies more weight and volume than carbon). However, some of the larger pores (and matrix microcracks) may be open to post-coat impregnations, and some of these openings may lead to deeper pores which, during subsequent high temperature excursions, can become accessible to liquefied SiO_2. While these sealants may trickle to varying degrees into the inner substrate porosity and even across the entire thickness, they are not intended to function as substrate densifiers, but as peripheral sealants. Silicate-based compounds will tend to flow around 1600°F (in contrast, the glassy carbon matrix is thermally inert). In addition, these sealants may introduce differential CTE problems within the surrounding matrix, and they can instigate decompositon reactions with substrate constituents. Their presence deep within the substrate porosity should be minimized. A 100% homogeneous glassy carbon matrix derived from a high carbonaceous, highly crosslinked polymer is the ultimate objective for both RCC and ACC.

Miscellaneous comments: Glassy carbon is more inert than most any carbon fiber (it is a hard, non-graphitizable carbon). Thus, during both the SiC conversion process and substrate oxidation events, the fibers will react first, then the matrix. The DTA modification was a great improvement for enhanced oxidation protection. Additionally, a second pyrolysis step might be considered after the second TEOS impregnation since trace releases of residual ethanol (and/or ethane plus water) may still be imminent. Sodium is a known catalyst for carbon oxidation. Trace residuals of Na^+ as well as any of the alkali and alkaline earth species can only represent bad news, especially if these oxidation catalysts become embedded within the substrate body after repeated Type A applications.

In many respects, RCC and ACC have much in common with other laminated, advanced composites within the industry. A prime example is the well known graphite/epoxy system now employed universally on a multitude of performance vehicles such as the mostly-composite F-22, JSF (F-35), F-117, B-2 and V-22 Tilt Rotor airplanes (some of my experience includes direct participation in the manufacturing and reliability areas of these programs). In many applications, these other vehicles do not see near the rigorous field conditions or harsh environments that carbon-carbon structures do. The majority of residual stresses that normally exist in composite articles on these other airplanes after their initial manufacturing process (stresses inadvertently incorporated into the part during the assembly process) rarely cause problems in the field (fortunately). The thermal and mechanical field loads these systems are subjected to are rather tame compared to the conditions RCC must repetitively endure. Over the years, many of the techniques developed during fabrication of 2-D laminated RCC (and PAN-based C-C forms as well) have progressively improved and many difficult problems have been resolved, particularly during the lay-up and composite fabrication stage. As-molded (non-pyrolyzed) RCC panels are quite robust and could offer some very valuable lessons learned to some of the other composite industries.

Unfortunately, 2-D laminated composites, in general, are plagued by limitations associated with the laminated nature of these systems. Experience has taught that poor nesting and meager ply-to-ply interactions lead to weak planes and weak planes are the prelude to most delaminations. However, this scenario (by itself) may not be necessarily related to the root cause of the RCC failures currently under investigation. It is more likely these failures are associated with thermal cycling fatigue in specific areas containing residual stresses (which develop into weak planes downstream) that are unintentionally incorporated into the part during the lay-up fabrication and/or coating processes as outlined in the previous report. It would be beneficial and rewarding to participate in a program of materials testing and physical/mechanical property correlations. In the long run, these efforts would lead to some vast improvements in RCC (and other C-C forms) in terms of performance capabilities and producibility. However, I wonder how much contribution this activity would practically provide in identifying the root cause of these current failures. Given the expected Shuttle retirement time frame, an aggressive manufacturing improvement initiative or long term property characterization program may not feasible or affordable. The failures in these particular panels at these specific WLE locations may well represent the first signs of aging deterioration and OML joggle coating spallation may only be one of the end-of-life events (or symptoms) manifested. The fault tree created for this investigation is quite comprehensive. Perhaps it is excessive for the particular failures under scrutiny. Identifying the exact failure mechanism here may or may not lead to a satisfying resolution of the issue at the program level. Personally, I would be more interested in determining where the next problems areas are going be. While these particular joggle regions may represent the weakest link in many instances, in other cases, the secondary or tertiary weak points may be the first ones to go. Successional failure points should be identified as soon as possible. With all the characterization that went into development and production of these panels, perhaps it is appropriate now to characterize their golden years. Identification and ranking of the top five or ten defects associated with LESS end-of-life material changes might be in order. Hopefully, the legacy of the Orbiter's RCC will provide inspiration for improved, next-generation versions of leading edge carbon-carbon platforms rather than the negative, inequitable perceptions which seem to have dominated the industry over the last two decades. There is little doubt that RCC was the original carbon-carbon material developed and applied in a major industrial endeavor and history has repeatedly proven that it is still the best carbon-carbon material around.

Appendix I

Table IA. Pyrolysis/impregnation/cure densification data (weight gains, weight losses and carbon gains) for 6-ply stemmed compression panels

NASA LaRC Task III Single Stem 6-Ply Compression Panels

Densification Data

Panel ID	% Weight Loss from Pyrolysis					% Weight Gain from Impregnation				% Carbon Weight Gain - Incremental				% Carbon Weight Gain - Cummulative			
1152-	As-Cured To ACC-0 η_{l0}	ACC-0B To ACC-1 η_{l1}	ACC-1B To ACC-2 η_{l2}	ACC-2B To ACC-3 η_{l3}	ACC-3B To ACC-4 η_{l4}	ACC-0 To ACC-0B η_{g0}	ACC-1 To ACC-1B η_{g1}	ACC-2 To ACC-2B η_{g2}	ACC-3 To ACC-3B η_{g3}	ACC-0 To ACC-1 $\eta_{c0\to1}$	ACC-1 To ACC-2 $\eta_{c1\to2}$	ACC-2 To ACC-3 $\eta_{c2\to3}$	ACC-3 To ACC-4 $\eta_{c3\to4}$	ACC-0 To ACC-1 $\eta_{c0\to1}$	ACC-0 To ACC-2 $\eta_{c0\to2}$	ACC-0 To ACC-3 $\eta_{c0\to3}$	ACC-0 To ACC-4 $\eta_{c0\to4}$
85	12.0	7.5	4.0	3.1	2.6	15.5	7.2	5.1	3.6	6.9	2.9	1.8	0.9	6.9	10.0	12.1	13.1
86	10.4	7.8	4.0	3.2	2.7	15.2	5.9	5.2	4.0	6.2	1.4	1.8	1.1	6.2	7.7	9.7	10.9
87	11.5	8.1	4.0	3.8	2.1	17.6	6.2	5.7	3.0	8.1	1.9	1.7	1.0	8.1	10.2	12.1	13.1
95	11.6	7.0	4.0	2.2	1.7	14.9	7.4	3.6	2.7	6.8	3.1	1.3	0.9	6.8	10.0	11.5	12.5
96	11.8	7.3	3.6	2.3	1.8	15.2	7.0	3.8	2.9	6.8	3.1	1.4	1.1	6.8	10.1	11.6	12.8
97	11.6	7.2	4.1	2.5	1.9	15.4	7.8	4.0	3.1	7.1	3.3	1.4	1.1	7.1	10.7	12.2	13.4
98	12.3	7.2	3.8	2.4	1.7	15.7	7.3	3.8	2.8	7.5	3.1	1.4	1.0	7.5	10.8	12.4	13.5
$\langle x \rangle$ =	**11.6%**	**7.4%**	**3.9%**	**2.8%**	**2.1%**	**15.6%**	**7.0%**	**4.5%**	**3.2%**	**7.1%**	**2.7%**	**1.5%**	**1.0%**	**7.1%**	**9.9%**	**11.7%**	**12.8%**
% σ =	5%	5%	4%	21%	20%	6%	10%	19%	15%	9%	27%	14%	9%	9%	10%	8%	7%

'B' = Bimatrix (impregnated/cured) state; i.e... matrix consists of both carbonized resin (glassy carbon) and cured impregnant resin (crosslinked phenolic polymer)

R[illegible]
1/87